Mechanisms of luminescence decay in YAG-Ce,Mg fibers excited by γ- and X-rays

A. Belsky, K. Lebbou, V. Kononets, O. Sidletskiy, A. Gektin, E. Auffray, D. Spassky, A.N. Vasil'Ev

Mechanisms of luminescence decay in YAG-Ce,Mg Fibers Excited by γ- and X-rays

A. Belsky [1,2*], K. Lebbou [1], V. Kononets [3], O. Sidletskiy [3], A. Gektin [3], E. Auffray [4], D. Spassky [5], A.N. Vasil'ev [5]

[1] *Institute of Light and Matter, UMR5306 CNRS, Université Lyon 1, Villeurbanne, France*
[2] *CELIA, Université de Bordeaux, CNRS, CEA, Talence, France*
[3] *Institute for Scintillation Materials, NAS of Ukraine, Kharkiv, Ukraine*
[4] *European Organization for Nuclear Research, Geneva 23, Switzerland*
[5] *Institute of Nuclear Physics, Moscow State University, Moscow, Russia*
[*] *Corresponding author*

Abstract

Time-resolved luminescence of YAG-Ce (150 ppm) fiber crystal with Mg co-doping was studied under pulsed X-ray excitation and γ-rays (Cs 662 keV). The initial part of decay kinetics under X-ray excitation is faster than for direct cerium excitation (63 ns). Decay kinetics is also characterized by the presence of slow components with at least two characteristic times longer than Ce^{3+} radiation time. The slowest one which dominates for t>500 ns in YAG-Ce without Mg co-doping practically vanishes for samples with 50 ppm co-doping. Decay kinetics under γ-rays are characterized by slower rise time than that under X-rays. These properties can be explained by competition of energy transfer and energy losses in track regions. The distribution of excitations in tracks produced by X-rays differs from that in tracks produced by γ-rays, since the energy of primary electron after γ-quantum conversion is much higher than after X-ray absorption. The stopping power for energetic electrons decreases with increase of electron energy, and therefore the density distribution after X-ray conversion is shifted to higher densities, Therefore, the acceleration of recombination and quenching of excitations is more prominent under X-ray excitation. Specific role of Ce^{4+} induced by Mg co-doping is also discussed in the paper.

Introduction

Relationships between the structure of excited region (track) formed by high energy particle or photon in a scintillator, and mechanisms of energy transfer from intrinsic electronic excitations to luminescence centers is important for understanding the processes in scintillators. Electronic excitations are distributed nonhomogeneously within a track, which may affect the light yield, luminescence rise and decay times, and energy resolution of a scintillator. Basing on the example of YAG-Ce, this paper discusses some aspects of energy transfer in activated

inorganic scintillators with account for inhomogeneous distribution of electronic excitation in tracks.

Influence of co-dopants on scintillation process has been extensively studied since 90th and during recent years [1-4]. Co-doping is a way to enhance light yield and accelerate luminescence decay.

There are two hypotheses on the role of divalent co-dopant in the modification of optical and scintillation properties of Ce-doped complex oxides. The first one claims that introduction of Mg^{2+} or Ca^{2+} leads to a concentration decrease of traps responsible for afterglow, and creation of new types of traps spatially correlated with Ce^{3+}, which makes carrier exchange between activator and host easier. The second hypothesis claims the relation of the ultraslow component weakening to the Ce^{4+} concentration increase at co-dopant addition [3, 4, 6]. It was suggested that Ce^{4+} ion is activated by the electron capture from the conductance band with subsequent photon emission by the formed $(Ce^{3+})^*$ ion.

In this work, the effect of Mg co-doping of YAG-Ce scintillator has been reconsidered basing on competition between energy transfer channels in regions with different concentration of electronic excitations.

Experimental

Samples of YAG-Ce (150 ppm) with Mg co-doping were grown using the micro-pulling-down technique [5]. The dopant values refer to the concentrations over yttrium sites. Chunks of YAG and YAG:Ce crystals produced by CRYTUR and Institute for Scintillation Materials NASU were used as raw materials. Raw materials were melted in iridium crucible and crystallized onto a YAG:Ce seed. Thermal gradients in the crystallizer were controlled by the iridium afterheater and alumina ceramic heat insulation. The pulling rate was 0.3 mm/hour. After growth the fibers were annealed in air at 1200 °C during 24 hours. As admixture segregation back to the melt is very weak in the micro-PD method, the Ce and Mg concentrations in melt and fiber are similar.

The luminescence of samples was studied under pulsed X-ray excitation, γ-rays (Cs 662 keV). For X-ray excitation we use Hamamatsu X-ray tube with the operating voltage 30kV, W anode, and 500 μm thick Be output window. Photocathode of this tube was excited by diode laser with the 50 ps pulse length and 200 kHz repetition rate (5 μs repetition period). Emission spectrum of such tube has maximum at 10 keV and is limited by Be transmission from the low energy side, and by anode voltage from the high energy side. Decay kinetics for Ce^{3+} emission was measured by fast PMT with spectral separation using interference filter with central wavelength of 560 nm and bandwidth of 20 nm. PMT signal together with synchronization signal from diode laser were inputs for PicoQuant Time-Correlated Single Photon Counting System. The time resolution of this system was about 200 ps. Decay signal of gamma scintillation was

detected by 9814QB PMT from ET Enterprises and measured using an 2 GHz oscilloscope with 1 ns sampling interval. A small percentage of the pulses was originating from single photoelectron noise of the PMT since very low trigger threshold was used to record the pulse shapes. Such events have been discarded and only the pulses from scintillation were used to calculate the average scintillation waveform. Scintillation kinetics of the samples was averaged over 1000 pulses.

Experimental results and discussion

At pulse X-ray irradiation with 5 μs repetition time T a slow luminescence decay component is clearly manifested with the much longer decay time compared to the pulse length. The constant level due to cumulative contribution of previous pulses is manifested in the measured decay curve for sample without co-doping (Fig. 1, blue curve, 0 ppm Mg). In case of periodic excitation, one should take into account the signals from all previous pulses. Therefore, this slow tail may be fit by a sum of hyperbolic functions $\sum_{n=0}^{\infty}(t+t_0+nT)^{-\alpha}$. The fitting gives $\alpha \approx 1.1$. The corresponding curve is plotted as green dashed line. This component is the main contribution into afterglow.

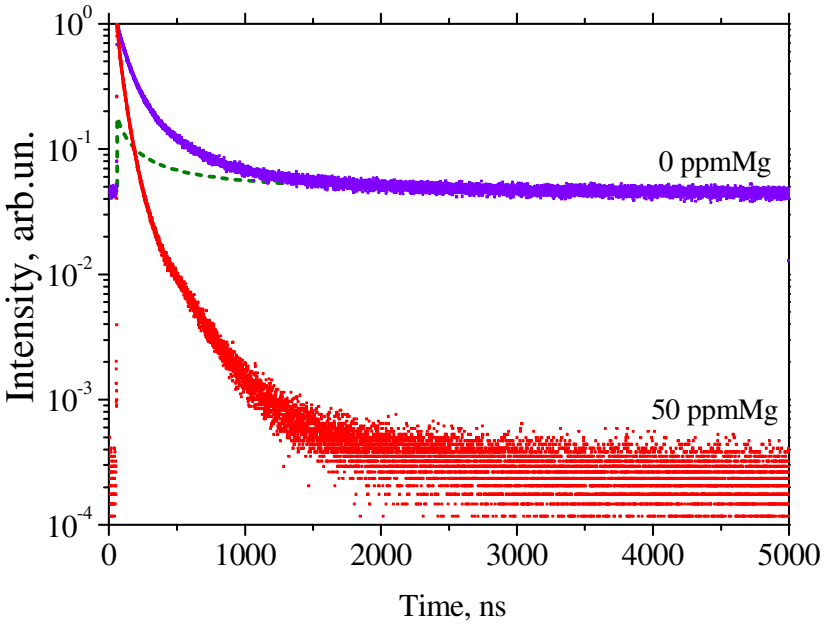

Fig. 1. Typical 560 nm luminescence decay curves of YAG-Ce (violet points,) and YAG-Ce,Mg (red points) under X-ray excitation. Green dotted line is the slow decay tail fitted by a sum of hyperbolic functions (see text).

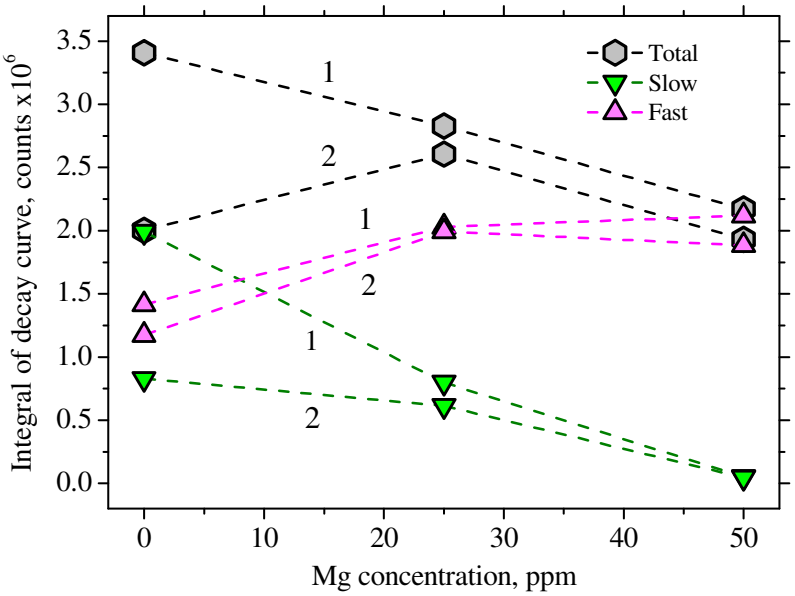

Fig 2. Decay curves integrated within the 5 μs repetition period of X-ray pulses for samples containing 0, 25, 50 ppm of Mg (gray hexahons – total integral), integral contribution from the ultraslow decay component (cumulative constant level) (green inverted triangles - Slow), scintillation component intensity, i.e. the difference between total and slow (magenta triangles - Fast). The samples were cut from fiber heads (1) and tails (2).

The quantitative estimations of the total YAG-Ce, Mg emission yield, ultraslow components and scintillation yield (integral of the decay over first 2 μs) are presented in Fig. 2 as a function on Mg concentration. With increasing Mg concentration, the contribution from the ultraslow component decreases by more than 10 times (green inverted triangles). In the Mg-free sample the latter constitutes about half of the overall luminescence yield. Meanwhile, it is different on heads and tails of the fiber. The scintillation component intensity (magenta triangles), which is the difference between total integral and integral of the cumulative constant level, remains about the same on both ends of the fiber at all Mg concentrations, and its contribution increases by about twice with Mg concentration increase from 0 to 50 ppm. One may conclude that defects are distributed nonuniformly along the fiber. Their concentration is higher near one of the fiber ends. The scintillation yield from both fiber sides is the same, it proves the efficiency of the μ-PD method for fabrication of scintillation elements. Study of about 10 samples with different Ce and Mg concentrations indicates that the slow component elimination occurs at the co-doping level about 50-100 ppm of Mg. As similar result was observed in other oxides doped with Ce or Pr, a mechanism of this phenomenon is, probably, the same.

The slow tail of emission is a negative factor both in fast-timing and scintillation applications. Even disregarding the hyperbolic tail, the decay kinetics under X-ray excitation differs significantly from single exponential law. Obviously, this decay curve shape is a result of competition between several mechanisms of Ce excitation. If we compare the decay curves under

X-ray excitation with decay under direct excitation of Ce^{3+} centers, we can see the difference both at short and long times. It is well-known that direct 410 nm excitation of 4f-5d_1 Ce^{3+} transition in YAG result in single exponential decay with intrinsic radiation time τ_R = 62 ns (see also Fig. 3 below). This time roughly corresponds to the middle part of the decay under X-ray excitation (see Fig. 1). The decay at short times show faster components, the appearance of which can be explained by the acceleration of kinetics after quenching of Ce^{3+} emission due to interaction with surrounding excitations. The appearance of components with characteristic times longer than intrinsic radiation time τ_R is related to additional intermediate stages of carrier transport (including carrier trapping) prior to energy transfer to Ce^{3+} ions.

Fitting the decay curve for the sample without co-doping by 3 exponentials within the initial 500 ns shows that the basic contribution comes from the components with the 80 ns (42%) and 300 ns (57%) decay times. The ultrafast component contribution with the decay time of about 10 ns is below 0.5 %.

Doping with 50 ppm Mg results in significant decrease of the slow contribution, and simultaneously in the decay acceleration at the initial stages (Fig. 1, red curve, 50 ppm Mg). A contribution from the ultrafast component increases up to 5%. The rest is distributed between the 50 ns (66 %) and 190 ns (29%) components. Another noted effect is the difference in scintillation decay measured under excitation of the same sample by X-rays and γ-rays. To illustrate this effect, Fig. 3 shows the initial 250 ns of Ce^{3+*} luminescence decay curves of Mg-co-doped sample (the same as shown in Fig. 1) for three types of excitation: direct excitation of the 4f-5d_1 transition in Ce^{3+} (measured using picosecond laser diode with 455 nm wavelength), excitation by ^{137}Cs γ-quanta, and photons emitted by X-ray tube. The direct excitation results in single exponential decay with the 62 ns characteristic time. As mentioned above, the luminescence decay kinetics is much more complicated under excitation with ionizing particles than under direct photoexcitation, and differs significantly for γ-quanta- and X-ray excitation. The initial part of decay curve under X-rays is faster to that at photoexcitation and characterized by decay 9 ns component. On the contrary, the rise-time of 5 ns is observed under gamma rays. Further trends of the decay curves are different as well: X-ray excited decay slows down and show 50 ns and 190 ns decay times, while the decay under γ-excitation is composed of two components 69 ns and 200 ns. The time resolution for both experimental setups was better than 1 ns. Therefore, we have to state that the balance of different energy transfer and cerium excitation mechanisms is significantly changed when the energy of exciting photon changes from 10 keV to 662 keV. This effect is general, but varies with parameters of hot relaxation of electronic excitations.

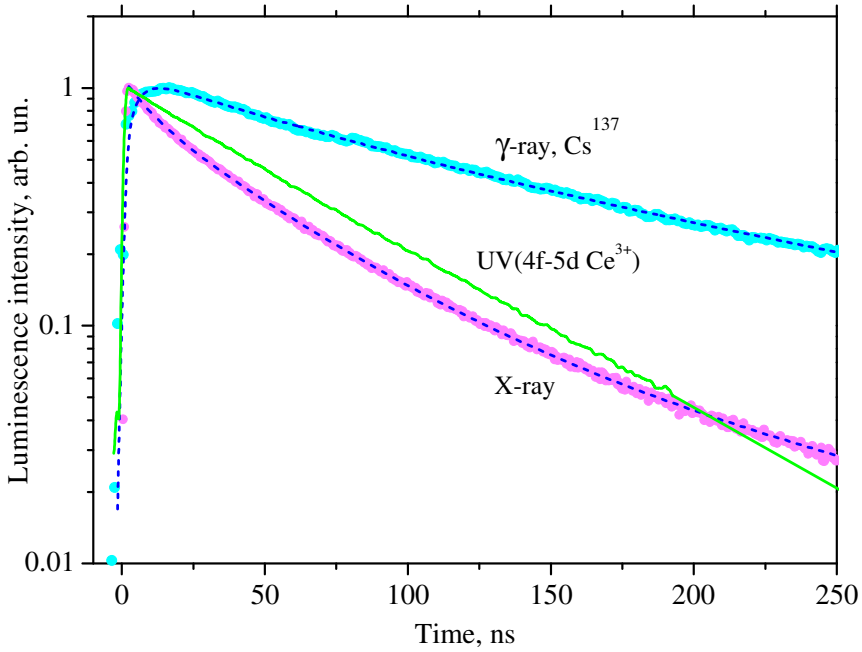

Fig. 3. YAG:Ce, Mg (50ppm) luminescence decay curves under gamma (blue), X-ray (magenta), and photo-excitation (green). Dashed curves are the result of fitting by three exponentials with characteristic times mentioned in the text.

The observed effects can be explained if one takes into account inhomogeneous distribution of electronic excitations in the track region and the difference of these distributions for γ and X-ray excitations.

It is well known that the luminescence efficiency and decay kinetics efficiency in scintillators and luminophores strongly depends on the concentration of thermalized excitations which defines energy transfer processes and competition between different channels of relaxation of electronic excitations (see, e.g. [7]). The distribution of carriers is essentially non-uniform in the track region, and therefore the decay of scintillation $I(t;E)$ can be estimated if we know the distribution of excitations and the luminescence response as a function of concentration [8, 9]:

$$I(t;E) = \int w(n;E)\, y(t;n)\, n\, d\log n\,,$$

where $y(t;n)$ is the time-dependent yield (per one excitation) of luminescence from the crystal with initial uniform concentration of excitations *n*. This yield can be estimated using the method of rate equations (see, e.g. [10]). To do so, the rate equations are solved separately for each of the excitation densities in the distribution. The distribution $w(n;E)$ of concentrations *n* over $\log n$ shows the fraction of the regions with concentration between *n* and $n(1+d\log n)$. This function

satisfies the conditions $\int w(n;E)\, d\log n = 1$, $\int w(n;E) n\, d\log n = N$, where $N(E)$ is the total number of excitations created by X-ray or γ-photon with energy E.

The spatial distribution of thermalized electronic excitations in the track region $w(n;E)$ can be estimated in the following way. During the first stage of interaction of primary electron with media this electron creates hot excitations along the electron path, and the linear density of energy deposit is the stopping power $-dE/dx$. This stopping power strongly increases with the slowing down of the primary electron, and therefore initial part of track has much lower linear density of electronic excitations. The higher the initial energy of primary electron, the longer the initial low-density part of track is. The range of 10 keV electron is about 1 μm, whereas the range of 662 keV electron 1 mm. So, the mean linear energy deposit along the track is about 20 times less for γ-photon than for X-ray photon. The cascade stage is finished faster than in 1 ps, and after this cascade all electrons and holes are distributed in energy in such a way that their kinetic energy is less than E_g. The thermalization of such electrons and holes due to phonon emission is accomplished by the shift of excitations from their birthplace. This shift is just 3D diffusion of the carriers along with thermalization. The spatial distribution is the convolution of Gaussians with the energy distribution of secondary excitations. This stage is described in details in [11]. When we convolve this 3D spread during thermalization with the 1D distribution of linear energy deposit along the track, we obtain spatial distribution of carriers in the track region. The distribution $w(n;E)$ can be calculated as the histogram of the concentrations using equidistant bins in $\log n$. This procedure is described in [8].

The results for calculation of excitation density distribution are presented in Fig. 4. A typical density distribution of created excitations spreads from 10^{10} to 10^{22} excitations per cm^3. The distributions of created excitation densities in YAG after absorption of gamma 662 keV photon (magenta curve A) are shifted to the lower concentration region in comparison with that for X-ray photon of 10 keV (blue curve B). The shift roughly corresponds to 20 times lower concentration (in accordance with the presented above estimation of linear energy deposit along the tracks). This increase of the weight of higher concentrations significantly modify the scintillation properties. The vertical lines in Fig. 4 separates the regions when electron and hole concentrations less or higher than the concentrations of cerium ions and defects considered in our simulation and expressed in ppm (measured in units of yttrium concentration). Vertical line 0 in Fig. 4 corresponds to the distance between excitations equal to dipole-dipole interaction radius.

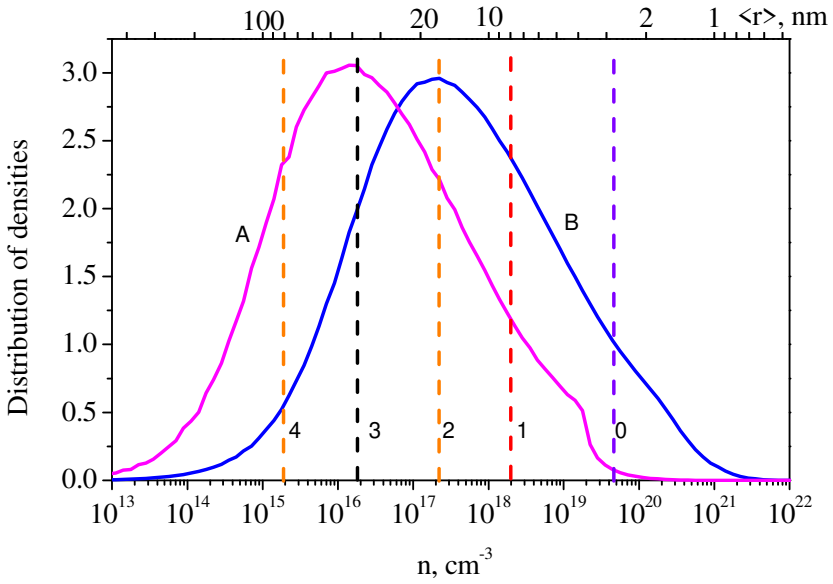

Fig.4. Excitation density distribution functions $w(n;E)$ for electron densities in the track in YAG at 300 K after absorption of γ-quantum (magenta curve A) and X ray photon of 10 keV (blue curve B). Vertical lines mark the concentrations of cerium ions and defects values considered in our simulation (1 – 100 ppm, 2 – 10 ppm, 3 – 1 ppm, 4 – 0.1 ppm) and 0 line corresponds to characteristic distance of dipole-dipole interaction between excitons resulting in the destroying of excitations. Top axis gives the mean distances between excitations.

The simplified scheme of recombination and capture processes should include at least three main processes. Two of them result in creation of excited cerium ion (1) due to the energy transfer from coupled electron-hole pair (exciton) to cerium ion Ce^{3+}, and (2) due to the capture of an isolated electron from the conduction band by Ce^{4+} ion. We suppose that the concentration of Ce^{4+} ions in YAG crystal increases with the increase of concentration of co-activator Mg^{2+} [3], and therefore the second process becomes more important in crystals with co-doping. The third important process is the capture of an electron by the trap followed by its release. After the delayed release the electron can be either captured by a hole and then pass the energy of the created exciton to the Ce^{3+} or can be captured by Ce^{4+} ion. In addition, we have to take into account the radiationless decay of excitations and migration of the charge carriers out of the track region.

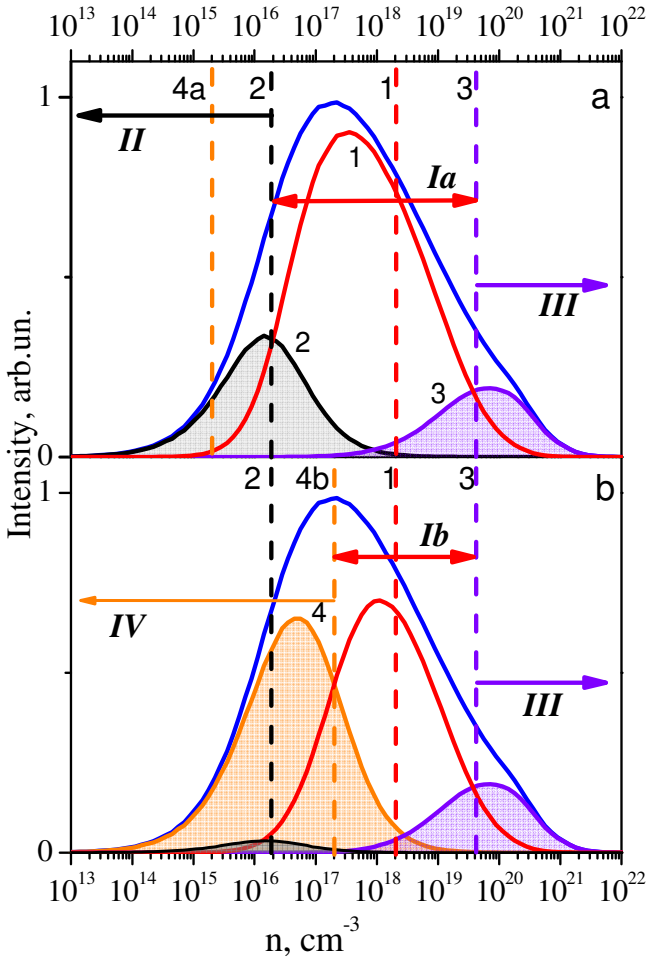

Fig. 5. Schematic presentation of number of excitations which pass through different recombination channels as functions of carrier concentration. Top panel (a) corresponds to low concentration of Ce^{4+} (the case of YAG-Ce), bottom panel (b) – corresponds to YAG-Ce, Mg, with 10% of Ce^{4+}. Density distribution for all electronic excitations created in the 10 keV X-ray track in YAG (blue curve); fraction of electrons which are captured by a hole with exciton creation and followed transfer to Ce^{3+} (red curve, 1); fraction of electrons captured by traps (black curve, 2); fraction of excitations which are destroyed due to interaction (violet curve, 3), fraction of electrons captured by Ce^{4+} (orange curve, 4). Vertical lines: 1 – Ce^{3+} concentration, 2 – concentration of traps, 3 – density of electronic excitations corresponding to quenching threshold, 4a,b – initial concentration of Ce^{4+}. Regions I to IV limited by dashed lines are discussed in text.

The fraction of different channels of recombination depending on the concentration of excitations is presented in Fig. 5 for YAG-Ce (top panel, a) and YAG-Ce,Mg (bottom panel, b). The fraction of each channel can be estimated as the ratio of the rate of this channel to the total rate of channels. For instance, an electron can be (1) captured by a trap with rate $w_{e+trap} \sim n_e n_{traps}$ proportional to concentration of traps n_{traps}, (2) captured by a Ce^{4+} ion with rate $w_{e+Ce^{4+}} \sim n_e n_{Ce^{4+}}$ proportional to concentration of traps $n_{Ce^{4+}}$, or (3) captured by a hole with rate $w_{e+h} \sim n_e n_h \approx n_e^2$

proportional to concentration of traps n_h. The latter process is preferable for high concentrations (it is bilinear in concentrations of electrons and holes), since initial concentration of holes is about concentration of electrons. Therefore, the fraction of electrons which are captured by, e.g. Ce^{4+} ions, equals to

$$\frac{w_{e+Ce^{4+}}}{w_{e+traps} + w_{e+Ce^{4+}} + w_{e+h}}$$

and decreases with increase of the concentration due to increase of w_{e+h}. This fraction multiplied by the number of excitations corresponding to n and $n(1+d\log n)$ interval is presented by orange curve 4 in Fig. 5b. All other curves in Fig. 5b are estimated in the same way. This approach is only qualitative, in order to get result quantitively one should solve the rate equations for all concentrations with precise knowledge of coefficients, which is the weak point in usage of rate equations.

In case of YAG-Ce the concentration of Ce^{4+} is small (we take it as 10^{-3} of the Ce^{3+} concentration), and the most probable reactions are (1) the creation of excitons followed by the energy transfer to Ce^{3+} [12] (region ***Ia***, $e+h \rightarrow ex$, $ex+Ce^{3+} \rightarrow Ce^{3+*}$), and (2) capture of electrons by traps followed by afterglow (region ***II***, e + trap $\rightarrow$ trap$^-$ $\rightarrow$ e + trap,). The first channel is fast whereas the second one is slow due to the slow release of electrons from traps. The first channel is realized in the track regions where the concentration of electronic excitations is higher than the concentration of traps. On the contrary, the regions of lower concentration of electronic excitations is characterized by the predominantly capture of electrons by traps. In this consideration we suppose that concentration of traps is 1% of the concentration of Ce^{3+}. For X-ray excitation about 20% of electron-hole pairs occur in the region ***II***. If we compare the shift of distributions between cases of X-ray excitation and γ-excitation (see Fig. 4), we see that for the latter case about 50% of e-h pairs occur in region ***II***. Moreover, high fraction of electronic excitations in the regions with their low concentration results in the observed long rise time for γ-excitation. Excitons in these regions are created after relatively long migration of electrons over traps. Therefore this migration results in the delayed excitation of Ce^{3+} ions and the increase of the emission time in the comparison with intrinsic radiation time of Ce^{3+*} centers. This rise time formation is similar to that observed under UV photoionization of cerium when the higher photon energy results in increase of the rise time due to increase of the thermalization length for electron with increase of its initial kinetic energy [13].

In the region of high concentration of electrons and holes (n>5×10^{18} cm^{-3}) excitons are created with high probability. But this region is characterized by high concentration of created excitons and therefore high probability of dipole-dipole interaction between excitons resulting in their death in Auger process ($ex+ex \rightarrow e+h$, recombination of one exciton results in transformation of the second one into energetic electron-hole pair due to Förster or Dexter energy transfer) [14]. The threshold for this process is shown in Fig. 5 by vertical line 3. In this region ***III*** excitons can be destroyed also due to interaction with electrons and holes, e.g. $ex+e \rightarrow e$ (Auger process when the energy of exciton is passed to the electron) [15]. The radiationless death of excitons occur

predominantly before the energy transfer to Ce^{3+}. This quenching results in the limitation of the light yield of YAG-Ce in comparison with theoretical limit. Please note that mentioned above processes of exciton quenching in regions of high concentration of excitations result only on decrease of scintillation yield without influence on the kinetics of cerium emission, since this quenching occurs prior to energy transfer to cerium.

Not only excitons can be quenched in regions of high concentration of other excitations. The excited cerium ions also can be quenched by free electrons, holes and excitons in these regions. Schematic presentation of interaction of excited cerium with excitons and electrons are shown in Fig. 6. These processes result in radiationless deexcitation of cerium (quenching) and reveal as the acceleration of decay with characteristic times shorter than cerium radiation time.

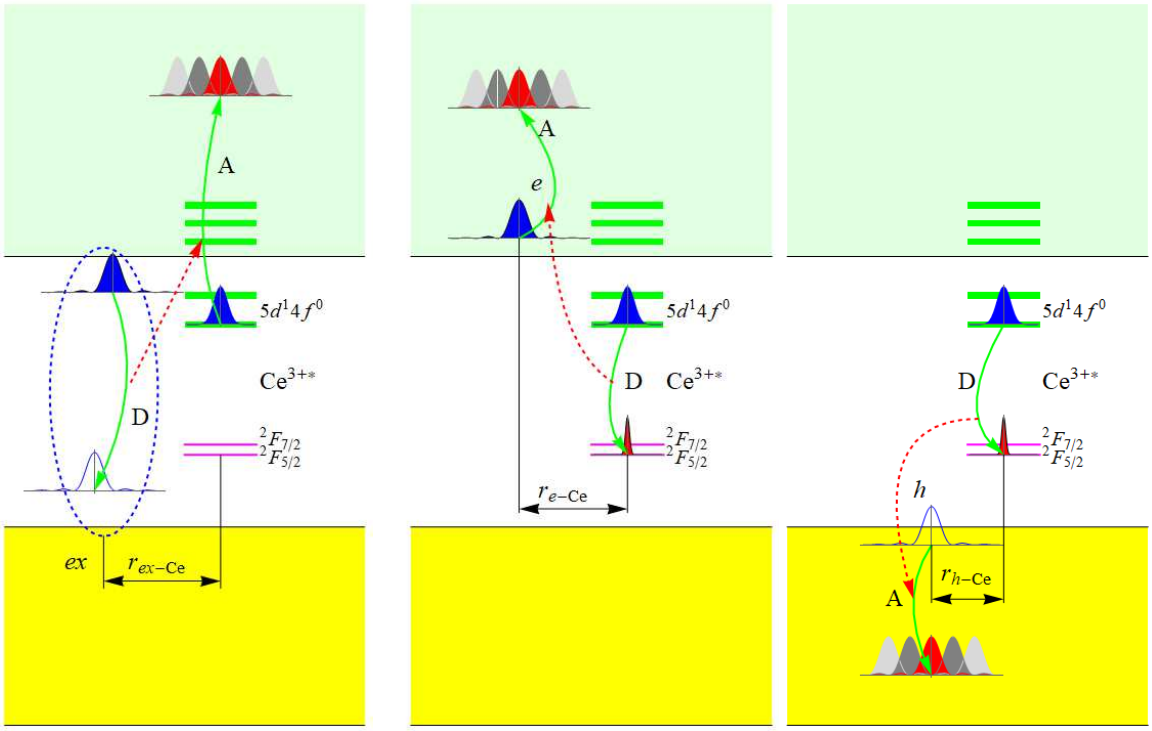

Fig. 6. Auger-type interaction of excited Ce^{3+*} with exciton resulting in Ce^{4+} and non-thermalized electron (left panel) and with electron resulting in deexcited Ce^{3+} and non-thermalized electron (middle). The process of de-excitation by hole is presented in right panel. These processes result in cerium deexcitation and decrease of the total number of electronic excitations. D – donor excitation, A – acceptor transition.

When we add Mg^{2+} co-doping, a part of Ce^{3+} is converted into Ce^{4+}. We consider the case when the resulting concentration of Ce^{4+} ions reaches 10% of Ce^{3+} (Fig. 5b). There is no effect of Mg^{2+} co-doping in the regions of high concentration of electronic excitations, whereas in regions of low and moderate concentration of excitations the role of Ce^{4+} is important. The capture of electrons by Ce^{4+} is more probable than the capture by traps since the concentration of Ce^{4+} is 10

times higher than the concentration of traps. Moreover, the capture cross-section for e+Ce^{4+} reaction is high due to Coulomb attraction. This results in the observed suppression of the long tails in kinetics, since the traps are not filled. Figure 5b shows that the region of concentrations for effective creation of excitons is narrower in comparison with Fig. 5a. Ce^{4+} ions can be effective in the regions of low concentration since they are converted into excited Ce^{3+*} states without migration over traps and without intermediate stage of exciton creation. Such centers can emit photons with cerium intrinsic radiation time. We use this process for the explanation of the decrease of decay components with characteristic time about hundreds of nanoseconds and increase of the components with 60 ns lifetime for crystals with Mg^{2+} co-doping. The presented discussion shows that about 10% of Ce^{4+} ions converted from Ce3+ ions results in the recombination of 30-40% of electronic excitations through this channel. This effect exists also for γ-excitation, but the decay kinetics in this case is still slower than for X-ray excitation due to the longer migration of electrons to cerium centers.

Many experiments show that the concentration of Mg above 1000 ppm results in the strong quenching of cerium emission resulting in the decrease of the yield and accelerating of kinetics in comparison with cerium radiation time. We also observe this effect (Fig. 1) but in our experiment Mg concentration does not exceed 50 ppm. We propose the following mechanism of the quenching of Ce^{3+*} emission when Ce^{4+} concentration is above 5% of Ce^{3+} concentration. After the capture of electrons by Ce^{4+} the excess holes are still existing in the valence band. Such non-equilibrium concentration of holes can exist only in samples with the presence of Ce^{4+}. The valence band is rather broad in oxides, its width for YAG is about 6 eV [16]. Therefore free hole can effectively quench Ce^{3+*} state due to Auger process h+Ce^{3+*}→h+Ce^{3+} when the cerium excitation passes to the hole with increase of its kinetic energy (thermalized hole from the top of the valence band goes deeper to the its bottom, see Fig.6, right panel). This quenching process results in the appearance of the decay components with characteristic time shorter than Ce^{3+*} radiation time, similar to the processes presented in Fig. 6. The distribution of concentration of electronic excitations for X-ray track is shifted to higher concentrations in comparison with γ-excitation, and holes are closer to Ce^{3+*} in the former case. Therefore the quenching is more prominent for X-ray excitation in case of high Mg^{2+} concentration. This result directly demonstrates the reasons of the quenching for high Ce^{4+} concentrations.

Conclusions

Samples YAG-Ce (150 ppm) with and without Mg co-doping were grown using micro-pulling-down technique [1]. The samples were studied under pulsed X-ray excitation (repetition period 5 μs, anode voltage 30 kV), γ-rays (Cs 662 keV).

Decay kinetics under X-ray excitation differs significantly from single exponential law. It is characterized by long hyperbolic tail $t^{-\alpha}$, $\alpha \approx 1.1$ at decay times much longer than cerium radiation time (63 ns). At short times the initial part of decay kinetics has decay faster than for direct

excitation. At the intermediate interval 100-500 ns the decay becomes faster with increase of Mg concentration. Slow component (long hyperbolic tail) which dominates in YAG-Ce without Mg co-doping for t>500 ns practically vanishes for samples with 50 ppm co-doping.

Decay kinetics under γ-rays also becomes faster with increase of Mg concentration. However, their profiles significantly differ from that observed under X-ray excitation. They are characterized by longer rise component of about 5 ns and slower decay in intermediate interval than under X-rays.

Using simulations described in [7-11] based on convolution of 1D linear distribution of secondary excitations along the track with 3D spatial distribution of thermalized excitations, this difference can be explained by the difference of the density distribution of excitations in the track region. The distribution under X-rays is shifted to higher densities due to much shorter range of primary electron, and this induces the acceleration of recombination and quenching. The analysis of the decay curves under X-ray and γ-excitation shows that most of excitation mechanisms involve the capture of an electron by Ce^{4+} ion, regardless of its nature (created during synthesis or created by ionization during excitation in the picosecond initial stages). The recombination kinetics is controlled by the distance between Ce^{4+} and electron and therefore depends on the density of excitations and mobility of electrons, which is controlled by the concentration and depth distribution of traps.

Aknowledgements

This research is carried out in the frame of Crystal Clear Collaboration and is supported by a European Union's Horizon 2020 research and innovation program under the Marie Skłodowska-Curie grant agreement No 644260 (INTELUM) and COST ACTION TD1401 (FAST). Authors kindly acknowledge Dr. V. Makhov and Dr. T. Syreishikova for measuring of characteristic decay time under direct excitation of Ce^{3+} in YAG-Ce,Mg fiber samples.

References

1. J. Barzowska, A. Kubicki, M. Grinberg, Acta Physica Polonica A 95 (1990) 395.
2. D. S. Hamilton, S. K. Gayen, G. J. Pogatshnik, R. D. Ghen, Phys. Rev. B 39 (1989) 8807.
3. Y. Wu, F. Meng, Qi Li, M. Koschan, C. L. Melcher, Phys Rev. Applied 2 (2014) 044009.
4. S. Blahuta, A. Bessière, B. Viana, P. Dorenbos, V. Ouspenski, IEEE Trans. Nucl. Sci. 60 (2013) 3134.
5. V. Kononets, K. Lebbou, O. Sidletskiy, Yu. Zorenko, M. Lucchini, K. Pauwels, E. Auffray, Springer International Publishing AG 2017 M. Korzhik and A. Gektin (eds.), Engineering of Scintillation Materials and Radiation Technologies, Springer Proceedings in Physics 200, p. 114,

6. M. Nikl, K. Kamada, V. Babin, J. Pejchal, K. Pilarova, E. Mihokova, A. Beitlerova, K. Bartosiewicz, S. Kurosawa, A. Yoshikawa, Crystal Growth & Design 14 (2014) 4827.
7. A. N. Vasil'ev, IEEE Transactions on Nuclear Science, 55 (2008) 1054.
8. A.N. Vasil'ev, Springer International Publishing AG 2017 M. Korzhik and A. Gektin (eds.), Engineering of Scintillation Materials and Radiation Technologies, Springer Proceedings in Physics 200, p. 3
9. A. Gektin, A. Vasil'ev, Radiation Measurements 122 (2019) 108.
10. S. Gridin, A. N. Vasil'ev, A. Belsky, N. Shiran, and A. Gektin, Physica Status Solidi (B): Basic Research 251 (2014) 942
11. A.N. Vasil'ev, A.V. Gektin, IEEE Transactions on Nuclear Science 61 (2014) 1054.
12. M. Kirm, A. Lushchik, Ch. Lushchik, G. Zimmerer, Physics and Chemistry of Luminescent Materials, eds. C. Ronda, L.E. Shea and A.M.Srivastava, PV 99-40, The Electrochemical Society Proceedings Series, Pennington, NJ (2000) pp. 113-122
13. A. Belsky, K. Ivanovskikh, A. N. Vasil'ev, M.-F. Joubert, Ch. Dujardin, J. Phys. Chem. Lett. 4 (2013) 3534.
14. C. Pedrini, B. Moine, D. Bouttet, A.N. Belsky, V.V. Mikhailin, A.N. Vasil'ev, E.I. Zinin, Chem. Phys. Lett. 206 (1993) 470.
15. A.N. Belsky, R.A. Glukhov, I.A. Kamenskikh, P. Martin, V.V. Mikhailin, I.H. Munro, C. Pedrini, D.A.Shaw, I.N. Spinkov, A.N. Vasil'ev, Journal of Electron Spectroscopy and Related Phenomena 79 (1996) 147.
16. http://aflow.org/material.php?id=Al5O12Y3_ICSD_93634

Figure captions

Fig. 1. Typical 560 nm luminescence decay curves of YAG-Ce (violet points,) and YAG-Ce,Mg (red points) under X-ray excitation. Green dotted line is the slow decay tail fitted by a sum of hyperbolic functions (see text).

Fig 2. Decay curves integrated within the 5 μs repetition period of X-ray pulses for samples containing 0, 25, 50 ppm of Mg (gray hexahons – total integral), integral contribution from the ultraslow decay component (cumulative constant level) (green inverted triangles - Slow), scintillation component intensity, i.e. the difference between total and slow (magenta triangles - Fast). The samples were cut from fiber heads (1) and tails (2).

Fig. 3. YAG:Ce, Mg (50ppm) luminescence decay curves under gamma (blue), X-ray (magenta), and photo-excitation (green). Dashed curves are the result of fitting by three exponentials with characteristic times mentioned in the text.

Fig.4. Excitation density distribution functions $w(n;E)$ for electron densities in the track in YAG at 300 K after absorption of γ-quantum (magenta curve A) and X ray photon of 10 keV (blue curve B). Vertical lines mark the concentration of cerium ions and defects values considered in our simulation (1 – 100 ppm, 2 – 10 ppm, 3 – 1 ppm, 4 – 0.1 ppm) and 0 line corresponds to characteristic distance of dipole-dipole interaction between excitons resulting in the destroying of excitations. Top axis gives the mean distances between excitations.

Fig. 5. Schematic presentation of number of excitations which pass through different recombination channels as functions of carrier concentration. Top panel (a) corresponds to low concentration of Ce^{4+} (the case of YAG-Ce), bottom panel (b) – corresponds to YAG-Ce, Mg, with 10% of Ce^{4+}. Density distribution for electronic excitations in the 10 keV X-ray track in YAG (blue curve); fraction of electrons which are captured by a hole with exciton creation and followed transfer to Ce^{3+} (red curve, 1); fraction of electrons captured by traps (black curve, 2); fraction of excitations which are destroyed due to interaction (violet curve, 3), fraction of electrons captured by Ce^{4+} (orange curve, 4). Vertical lines: 1 – Ce^{3+} concentration, 2 – concentration of traps, 3 – density of electronic excitations corresponding to quenching threshold, 4a,b – initial concentration of Ce^{4+}. Regions I to IV limited by dashed lines are discussed in text.

Fig. 6. Auger-type interaction of excited Ce^{3+*} with exciton resulting in Ce^{4+} and non-thermalized electron (left panel) and with electron resulting in deexcited Ce^{3+} and non-thermalized electron (right). Both processes result in cerium deexcitation and decrease of the total number of electronic excitations.